

## Pion-induced pion production in nuclei

F. Bonutti,<sup>1,2</sup> P. Camerini,<sup>1,2</sup> E. Fragiaco,<sup>1,2</sup> N. Grion,<sup>1</sup> R. Rui,<sup>1,2</sup> J. T. Brack,<sup>3,8</sup> L. Felawka,<sup>2</sup> E. F. Gibson,<sup>6</sup> G. Hofman,<sup>3,4</sup> M. Kermani,<sup>3,4</sup> E. L. Mathie,<sup>5</sup> S. McFarland,<sup>3,4</sup> R. Meier,<sup>3</sup> D. Ottewell,<sup>3</sup> K. Raywood,<sup>3</sup> M. E. Sevier,<sup>7</sup> G. R. Smith,<sup>3</sup> and R. Tacik<sup>5</sup>

<sup>1</sup>*Istituto Nazionale di Fisica Nucleare, 34127 Trieste, Italy*

<sup>2</sup>*Dipartimento di Fisica dell'Universita' di Trieste, 34127 Trieste, Italy*

<sup>3</sup>*TRIUMF, Vancouver, British Columbia, Canada V6T 2A3*

<sup>4</sup>*Physics Department, University of British Columbia, Vancouver, British Columbia, Canada V6T 2A6*

<sup>5</sup>*University of Regina, Regina, Saskatchewan, Canada S4S 0A2*

<sup>6</sup>*California State University, Sacramento, California 95819*

<sup>7</sup>*School of Physics, University of Melbourne, Parkville, Victoria, 3052, Australia*

<sup>8</sup>*University of Colorado, Boulder, Colorado 80309*

(The CHAOS Collaboration)

(Received 19 December 1996)

The process of pion-induced pion production in nuclei has been studied with the  $A(\pi^+, \pi^+ \pi^-)$  and  $A(\pi^+, \pi^+ \pi^- p)$  reactions for four nuclei  ${}^2\text{H}$ ,  ${}^{12}\text{C}$ ,  ${}^{40}\text{Ca}$ , and  ${}^{208}\text{Pb}$  at an incident pion energy of  $T_{\pi^+} = 283$  MeV. The  $\pi^+ \pi^-$  and  $\pi^+ \pi^- p$  particles in the final state were detected in coincidence with the CHAOS spectrometer at TRIUMF. By looking at kinematic quantities such as missing momentum and missing energy, we have been able to draw some model-independent conclusions about the dynamics of the  $\pi \rightarrow \pi\pi$  process in nuclei, which do not vary significantly with target mass. We find that the incident pion interacts mainly with one surface nucleon via the leading  $\pi N \rightarrow \pi\pi N$  channel. The pion pair releases no appreciable energy to the residual nucleus, which remains substantially bound throughout the reaction. These findings underline the quasifree nature of the pion production reaction in nuclei. [S0556-2813(97)00605-5]

PACS number(s): 25.80.Hp, 13.75.Gx

### I. INTRODUCTION

In the field of pion physics at intermediate energy, the experimental investigation of the pion production process in nuclei has received poor attention. Before the advent of the meson factories (LAMPF, SIN/PSI, and TRIUMF), there are only a few reported results from measurements on emulsions, dealing mainly with total cross sections [1]. These data have a poor statistical significance and the premeson factory database was able to give only a marginal idea of the dynamics of the pion production process in nuclei. The better quality and the more intense fluxes of pion beams delivered by the meson factories have slightly improved the  $\pi A \rightarrow \pi\pi A'$  database: there are four data points on the  $A$  dependence, and one datum on the  $T$  dependence [2] of the total cross sections, and a few articles which address two peculiar aspects of the di-pion dynamics in nuclear matter [3–5].

The most recent work [6] examined the  $A$  dependence of  $\pi^+ \pi^+$  and  $\pi^+ \pi^-$  invariant mass spectra, measured in the  $A(\pi^+, \pi^+ \pi^\pm)$  reaction at  $T_{\pi^+} = 282.7$  MeV. It was found that the shapes of the mostly  $J=0$ ,  $I=2$   $\pi^+ \pi^+$  spectra did not vary significantly with  $A$ , while the mostly  $J=I=0$   $\pi^+ \pi^-$  spectra showed an enhancement near the  $2m_\pi$  threshold, which increased dramatically with increasing  $A$ . This behavior can be attributed to nuclear-medium modifications of meson properties. Such studies provide a useful tool for understanding meson dynamics in a nuclear many-body environment and, consequently, the relevant degrees of free-

dom which should be used to describe it [7].

A nuclear medium is characterized simply by its density  $\rho$ . For  $\rho \leq \rho_n = 0.16 \text{ fm}^{-3}$  (the nuclear saturation density), the meson mass distribution is predicted [8] to be modified by the density of the nuclear environment for  $\pi\pi$  pairs interacting in the  $J=I=0$  channel, and such a modification of the mass distribution can be observed experimentally since it occurs at  $\rho < \rho_n$ , i.e., in conventional nuclei. A similar modification of the mass distribution is predicted in the  $J=I=1$  channel, but only at the experimentally inaccessible density of  $\rho \approx 1.5\rho_n$ .

In this article, we extend the analysis presented in Ref. [6] for the  $A(\pi^+, \pi^+ \pi^-)$  reaction, and report on new results on the semiexclusive  $A(\pi^+, \pi^+ \pi^- p)$  reaction. The experiment was performed at TRIUMF by using the CHAOS spectrometer [9]. This facility is particularly suited to detect events with many charged particles in the final state, and this performance was fully exploited in the present measurement. The targets studied were  ${}^2\text{H}$ ,  ${}^{12}\text{C}$ ,  ${}^{40}\text{Ca}$ , and  ${}^{208}\text{Pb}$ , at an incident pion energy of  $T_{\pi^+} = 282.7$  MeV.

The pion production data have been analyzed and reduced to common kinematical quantities: missing momentum, missing energy, and proton kinetic energy. The distributions of these quantities do not require, by their nature, a direct comparison with the predictions of models to understand the underlying physics. Thus, conclusions eventually drawn are *model independent*. The specific dynamical features of the pion production process addressed in this article are (1) How many nucleons are involved in the initial pion production

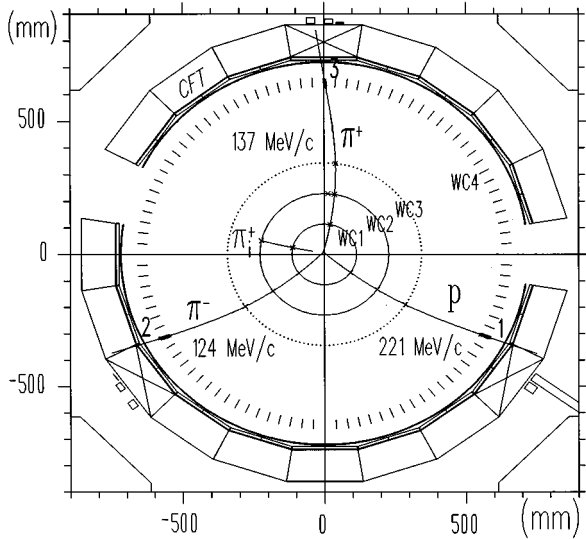


FIG. 1. Top view of CHAOS and a typical  $\pi_i^+ A \rightarrow \pi^+ \pi^- p [A-1]$  event.  $\pi_i^+$  indicates the incoming beam pion that has induced the reaction. The four circles correspond to the cylindrical wire chambers (WC), the outermost being a drift chamber (WC4). WC4 is surrounded by 20 CFT's, the CHAOS fast trigger telescopes. In order to free the pion beam path, two of them are removed from CHAOS. CFT's are also used for particle mass identification. The telescopes which have recorded an event are marked with crosses. The boxes behind them have a height proportional to the response functions in the three telescope layers. The square external frame represents the inside dimensions of the magnet dipole; units are in mm.

reaction? (2) Where does the interacting nucleon lie in the nucleus? (3) Is the pion-pair propagation strongly influenced by the presence of the nuclear environment? (4) How does the production process depend on the (average) density of the nuclear environment?

## II. EXPERIMENT

The experiment was performed at the CHAOS spectrometer facility of TRIUMF by using the medium energy pion beam M11. The incident pion beam had a central momentum of 398.5 MeV/c and a momentum width of 1.2% ( $\sigma$ ). The intensity was  $4 - 5 \times 10^6 \pi^+/s$  at the target spot. These working conditions were kept constant throughout the data-taking phase of the experiment.

### A. CHAOS spectrometer

The CHAOS magnetic spectrometer [10] consists of a dipole magnet, four concentric cylindrical wire chambers, and a system of 20 counter telescopes that surround the magnet poles. Targets, either cryogenic or solid, are accommodated at the central vertical axis of the magnet.

A typical  $\pi_i^+ A \rightarrow \pi^+ \pi^- p [A-1]$  event is displayed in Fig. 1. The proportional wire chambers WC1 and WC2 record the passage of the incident pion (labeled  $\pi_i^+$  in Fig. 1). These chambers, along with the drift chambers WC3 [11] and WC4, are also used to reconstruct the trajectories of particles emerging from the target. WC3 and WC4 are dead-

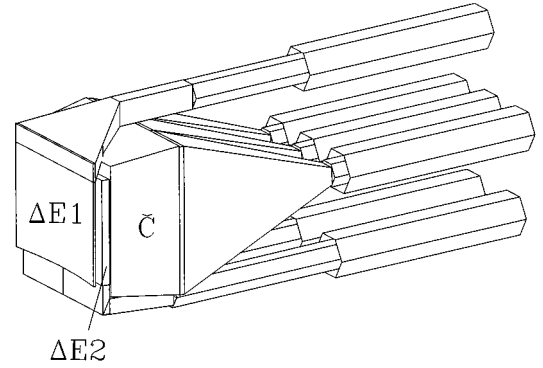


FIG. 2. ACAD representation of a CHAOS fast trigger (CFT) telescope.  $\Delta E1$  and  $\Delta E2$  are NE110 plastic scintillators 3 mm and 12 mm thick, respectively. The 20 adjacent  $\Delta E1$  counters define the geometric solid angle of CHAOS, which is 1.5 sr.  $\Delta E1$  is a cylindrical segment of radius 710 mm, 178 mm high.  $\Delta E2$  consists of two distinct rectangular counters 180 mm high.  $\check{C}$  is a SF5 lead-glass block coupled to three photomultipliers through plexiglass light guides. It is used as a Cerenkov counter.

ened in the regions traversed by the pion beam, because of the intense pion flux used. The spatial resolution of the wire chambers, with the magnetic field set at 0.5 T, resulted in a typical momentum resolution of 2% ( $\sigma$ ).

Particles are mass identified by using the CHAOS fast trigger telescopes (CFT) [12]. Each CFT telescope (illustrated in Fig. 2) consists of three layers: the first two layers,  $\Delta E1$  and  $\Delta E2$ , are NE110 plastic scintillator counters used as differential energy counters, the third layer is a SF5 lead-glass counter ( $\approx 5\chi_0$  thick) used as a Cerenkov counter. Twenty adjacent telescopes cover  $360^\circ$  in the reaction plane, however, the two CFT telescopes which intercept the pion beam are removed from CHAOS during the actual experiment.

The coincidence between an incident pion signal ( $S_{\pi_i^+}$ ) and at least two signals from distinct CFT's defines the first level trigger (FLT). That is, a FLT signal is generated every time the  $S_{\pi_i^+} \times \prod_{i=1}^2 (\Delta E1 \times \Delta E2)_i$  logic condition is satisfied. The FLT signal enables the electronics of the second level trigger (SLT) [13] which is designed to use information from the three innermost chambers to reconstruct particle tracks, i.e., to calculate particle momentum, polarity, and distance of closest approach to the target center. This track information is then used to accept or reject an event. The decision is made in a very short time, typically in few  $\mu s$ , depending on the number of detected tracks. In the present experiment, the SLT was required to have either two tracks of opposite polarity, or three tracks emanating from within a fixed distance of the target center. These requirements drastically reduced the number of events passed to the data acquisition system, and eventually recorded on tape for off-line analysis. Typically, for an incoming beam rate of about  $4 \times 10^6 \pi^+/s$ , the number of events passing the FLT and SLT was 4000/s and 60/s, respectively. Finally, out of these 60, 50 events/s were recorded on tape, for a dead time of about 15%.

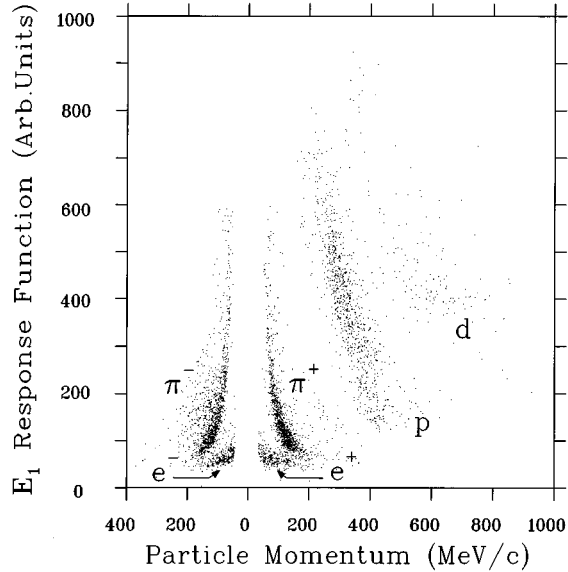


FIG. 3. Diffusion plot of the  $\Delta E1$  response function versus the particle momentum. The particle mass separation has been enhanced by placing constraints on the particle polarity and the particle response functions in the other two elements of a CFT.

### B. Targets

The targets used in this experiment were  $^2\text{H}$ ,  $^{12}\text{C}$ ,  $^{40}\text{Ca}$ , and  $^{208}\text{Pb}$ . The  $^2\text{H}$  target consisted of a cylinder, 5 cm in diameter by 5 cm in height, containing liquid deuterium. The remaining ones were solid targets of thicknesses  $0.332\text{ g/cm}^2$  for  $^{12}\text{C}$ ,  $0.180\text{ g/cm}^2$  for  $^{40}\text{Ca}$ , and  $0.604\text{ g/cm}^2$  for  $^{208}\text{Pb}$ .

### C. Particle mass identification

In the pion production reaction, a particle track was characterized by two quantities: the particle vector momentum and the particle response functions in the CFT layers. All these quantities were used to identify it. Figure 3 shows a diffusion plot of the response functions in  $\Delta E1$  of  $e$ ,  $\pi$ ,  $p$ , and  $d$  versus their momentum. In order to enhance the particle mass selectivity, the  $\Delta E1$  response function was filtered with the particle response functions in the other two CFT layers and with the particle polarity. Use of this approach in the present experiment resulted in a particle ( $e$ ,  $\pi$ ,  $p$ , and  $d$ ) mass identification efficiency of 98% [12].

During data reduction some soft kinematical cuts were applied to particle momenta (energies) and angles. Events were rejected when a particle, identified either as a pion or as a proton, had a momentum which exceeded the values allowed by the  $A(\pi^+, \pi^+ \pi^- p)[A-1]$  reaction phase space. In addition, events were rejected for  $\pi^+ \pi^-$  opening angles below  $2^\circ$ ; in this case,  $e^+ e^-$  pairs may emulate  $\pi^+ \pi^-$  pairs. The  $e^+ e^-$  pairs come from  $\pi^0$  decays, and subsequent  $\gamma$  conversion in the target region. The above limitations have a negligible effect on the phase-space volume of the pion production reaction, while improving the degree of accuracy for particle mass discrimination to nearly 100%. The particle momentum (energy) and angle limits are listed in Table I.

TABLE I. Soft limitations on kinematical quantities for pions and protons. Events, after being mass identified, are accepted if they fall within the ranges specified in the table. The notations  $p_{\pi^\pm}$ ,  $T_{\pi^+} + T_{\pi^-} + T_p$ , and  $\theta_{\pi^+ \pi^-}$  indicate the pion momenta, the particle energy sum, and the pion pair opening angle, respectively. Protons are rejected if their momenta are below the CHAOS threshold, which is  $187\text{ MeV}/c$ . The CHAOS threshold for pions is  $55\text{ MeV}/c$ .  $T_{\text{thr}}$  is the CHAOS threshold for either pions or protons.

	$p_{\pi^\pm}$ (MeV/c)	$T_{\pi^+} + T_{\pi^-} + T_p$ (MeV)	$\theta_{\pi^+ \pi^-}$ (deg)
$^2\text{H}$	55 – 205	$T_{\text{thr}} - 140$	2 – 178
$^{12}\text{C}$	55 – 195	$T_{\text{thr}} - 140$	2 – 178
$^{40}\text{Ca}$	55 – 195	$T_{\text{thr}} - 145$	2 – 178
$^{208}\text{Pb}$	55 – 200	$T_{\text{thr}} - 145$	2 – 178

## III. ANALYSIS

### A. Description of the kinematical variables

The measured pion and proton vector momenta were combined and reduced to common kinematical variables, with only energy and momentum conservation. These variables are discussed in detail below.

*Recoil momentum.* This is the momentum of the residual nucleus in the  $A(\pi^+, \pi^+ \pi^- p)[A-1]$  reaction. In the exit channel, the  $[A-1]$  nucleon system is undetected, thus, the calculated recoil momentum simply refers to an  $[A-1]$  nucleon system, whether it is bound or unbound.

*Missing energy.* For the  $A(\pi^+, \pi^+ \pi^- p)[A-1]$  reaction, the missing energy is defined by the equation

$$\begin{aligned}
 E_M &= E_{A-1}^* + T_{A-1} \\
 &= [M_A - M_{A-1} - m_\pi - m_p] - [T_{\pi^+}^f + T_{\pi^-}^f + T_p - T_{\pi^+}^i],
 \end{aligned} \tag{1}$$

where  $M_A$ ,  $M_{A-1}$ ,  $m_\pi$ , and  $m_p$  are the masses of the target nucleus, residual nucleus, pion, and proton, respectively. The quantities  $T_{\pi^+}^i$ ,  $T_{\pi^+}^f$ ,  $T_{\pi^-}^f$ ,  $T_{A-1}$ , and  $T_p$  are the kinetic energies of the incident pion, the two final pions, the residual nucleus, and the proton, respectively.  $E_{A-1}^*$  accounts for the energy necessary to remove a nucleon from a single orbital, and to excite the residual nucleus. The nucleus  $[A-1]$  can de-excite either by emitting  $\gamma$  rays,  $[A-1]^* \rightarrow [A-1] + \gamma$ , or a nucleon,  $[A-1]^* \rightarrow [A-2] + N$ , when the excitation energy exceeds the  $N$  binding energy. In this case,  $M_{A-1} < M_{A-2} + M_N$ , and  $E_M$  calculated with Eq. (1) overestimates the result. These energies are folded into the measured missing energy distributions because of the moderate resolution of the experimental apparatus. Thus, the  $E_M$  distributions are expected to appear as broad peaks. Since  $T_{A-1} \simeq 0\text{ MeV}$ , Eq. (1) simplifies to

$$E_M \simeq E_{A-1}^*. \tag{2}$$

This approximation derives from the low magnitude of the  $[A-1]$  recoil momentum, which does not exceed  $400\text{ MeV}/c$  for the examined nuclei, as will be seen in Fig. 4.

*Proton energy.* This quantity is determined by the proton momentum which, for the  $A(\pi^+, \pi^+ \pi^- p)[A-1]$  reaction

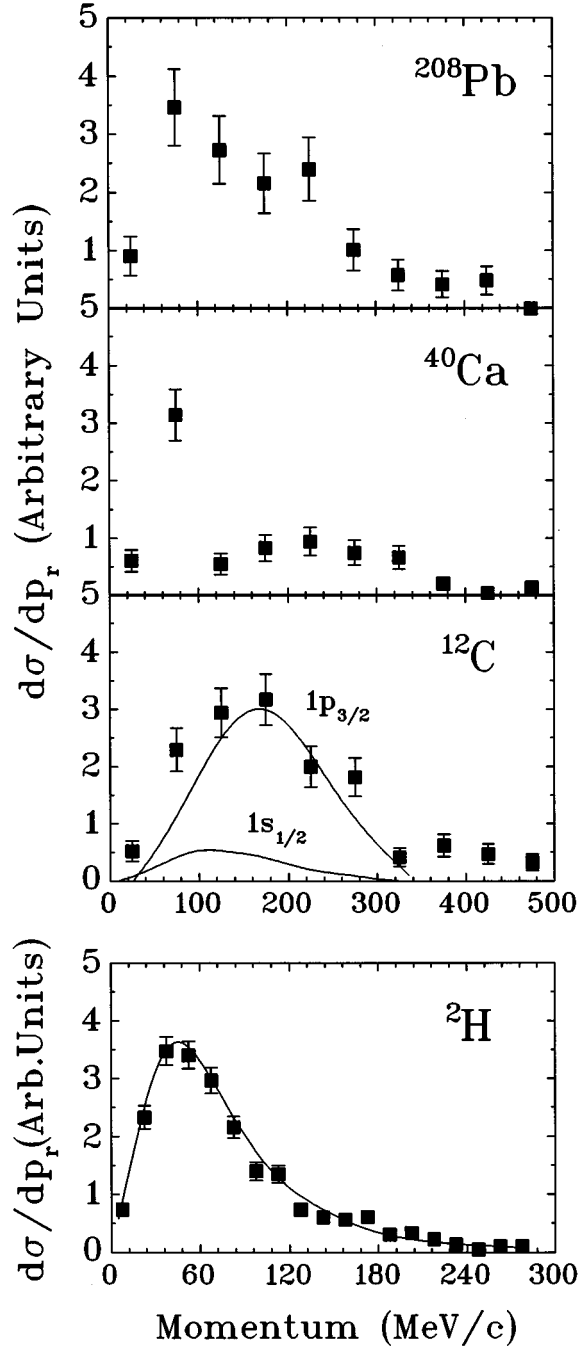


FIG. 4. Recoil momentum distributions for the  $A(\pi^+, \pi^+ \pi^- p)[A-1]$  reaction (full squares). The solid lines are taken from the  ${}^2\text{H}(e, e' p)n$  data of Ref. [14], and the DWIA calculation of Ref. [15] for the  $1s_{1/2}$  and  $1p_{3/2}$  proton knock out in the  ${}^{12}\text{C}(e, e' p)$  reaction.

channel, is directly measured by CHAOS. The proton energy can be also derived by measuring the kinetic energies of the two final pions in the  $A(\pi^+, \pi^+ \pi^- p)[A-1]$  reaction channel. If the  $[A-1]$  nucleon system is assumed to stay bound, then the proton energy becomes

$$T_p = [M_A - M_{A-1} - m_{\pi^-} - m_p] - [E_{A-1}^* + T_{A-1}] - [T_{\pi^+}^f + T_{\pi^-}^f - T_{\pi^+}^i]. \quad (3)$$

TABLE II. Widths and shifts of the missing energy ( $E_M$ ) distributions for the  $A(\pi^+, \pi^+ \pi^- p)[A-1]$  reaction.  $\sigma_{E_M}$  is the Gaussian half-width (obtained by fitting the measured  $E_M$  distributions in Fig. 5) and  $\sigma_{E_M}^i$  is the instrumental half-width [calculated with Eq. (5)].  $\mu_{E_M}$  is the mean-value of the  $E_M$  distributions. In the case of deuterium, the proton mass is subtracted.

	$\sigma_{E_M}$ (MeV)	$\sigma_{E_M}^i$ (MeV)	$\mu_{E_M}$ (MeV)
${}^2\text{H}$	7.6	7.5	$0.70 \pm 0.01$
${}^{12}\text{C}$	8.4	7.8	$5.0 \pm 0.2$
${}^{40}\text{Ca}$	12.0	7.6	$3.7 \pm 0.3$
${}^{208}\text{Pb}$	14.8	8.1	$9.5 \pm 0.6$

In the data reduction  $T_{A-1}$  was taken equal to 0 MeV and  $E_{A-1}^*$  was replaced by its mean value ( $\mu_{E_M}$ ) whose values are reported in Table II.

### B. Data analysis and reduction

The vertical error bars shown with the data points in Figs. 4–6 represent only statistical uncertainties. There is an additional systematic error due to the applied correction for the irregular CHAOS acceptance. This has been calculated to  $\approx 10\%$  with a GEANT simulation of CHAOS. Other systematic errors are negligible since the distributions are presented in arbitrary units.

There are uncertainties associated with the kinematical variables discussed above due to momentum measurements associated with the M11 pion beam and the CHAOS spectrometer. For the proton energy distributions shown in Fig. 6, the error sizes are obtained by using Eq. (3), and are indicated by horizontal error bars. The widths of the  $E_M$  distributions shown in Fig. 5 reflect both the instrumental uncertainty  $\sigma_{E_M}^i$  in determining  $E_M$  and the uncertainty  $\sigma_{E_M}^{A-1}$  in establishing the mass of the  $[A-1]$  system of nucleons.

$$(\sigma_{E_M})^2 = (\sigma_{E_M}^{A-1})^2 + (\sigma_{E_M}^i)^2. \quad (4)$$

Experimental results indicate that the  $[A-1]$  system of nucleons stays preferentially bound, thus  $\sigma_{E_M} = \sigma_{E_M}^i$ . However, when the residual nucleus decays by emitting a nucleon  $\sigma_{E_M} > \sigma_{E_M}^i$ .

The variance  $(\sigma_{E_M}^i)^2$  for  $E_M$  can be expressed in terms of the variances  $\sigma_{T_{\pi^+}^i}^2$ ,  $\sigma_{T_{\pi^\pm}^f}^2$  and  $\sigma_{T_p}^2$  for the variables  $T_{\pi^+}^i$ ,  $T_{\pi^\pm}^f$  and  $T_p$  which were actually measured:

$$(\sigma_{E_M}^i)^2 = (\sigma_{T_{\pi^+}^i})^2 + (\sigma_{T_{\pi^\pm}^f})^2 + (\sigma_{T_{\pi^\pm}^f})^2 + (\sigma_{T_p})^2. \quad (5)$$

The magnitude of  $(\sigma_{E_M}^i)^2$  in Eq. (5) is determined mainly by  $(\sigma_{T_{\pi^+}^i})^2$  and  $(\sigma_{T_p})^2$ . The standard deviation  $\sigma_{T_p}$  accounts for both the uncertainty in measuring the proton energy with CHAOS and the proton energy loss in the target. The uncertainty in the latter quantity cannot be eliminated for the solid targets, since the spatial resolution of the spectrometer is comparable with the target thicknesses. Thus, the particle energy losses in the targets were simulated with a Monte

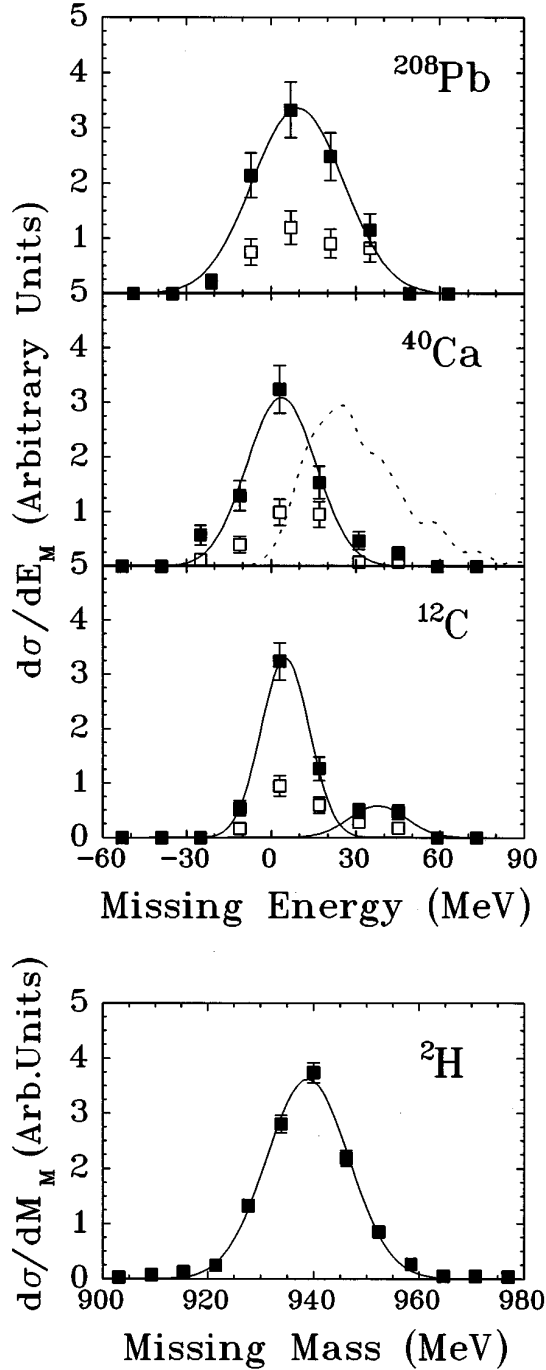


FIG. 5. Missing mass and energy distributions, in arbitrary units, for the  $A(\pi^+, \pi^+ \pi^- p)[A-1]$  reaction. The  $[A-1]$  residual nucleus is assumed to be bound. The solid lines are Gaussian best fits of the distributions. In the  ${}^2\text{H}$  plot, the data represent the missing mass of the residual nucleus, a proton. In the  ${}^{12}\text{C}$ ,  ${}^{40}\text{Ca}$ , and  ${}^{208}\text{Pb}$  plots, the missing energy distributions are for  $M_{\pi^+ \pi^-} \geq 2m_\pi$  (full squares), and for  $2m_\pi \leq M_{\pi^+ \pi^-} \leq 315$  MeV (open squares),  $M_{\pi^+ \pi^-}$  being the  $\pi^+ \pi^-$  invariant mass. The dotted line is a phase-space simulation of the missing energy distribution for the  ${}^{40}\text{Ca}(\pi^+, \pi^+ \pi^- p){}^{38}\text{K}$  reaction.

Carlo code. In order to check the consistency of the simulations,  $\sigma_{E_M}^i$  was calculated and compared to the measured standard deviation  $\sigma_{E_M}$ . The values of  $\sigma_{E_M}$  and  $\sigma_{E_M}^i$  are reported in Table II, as well as the mean value of the  $E_M$

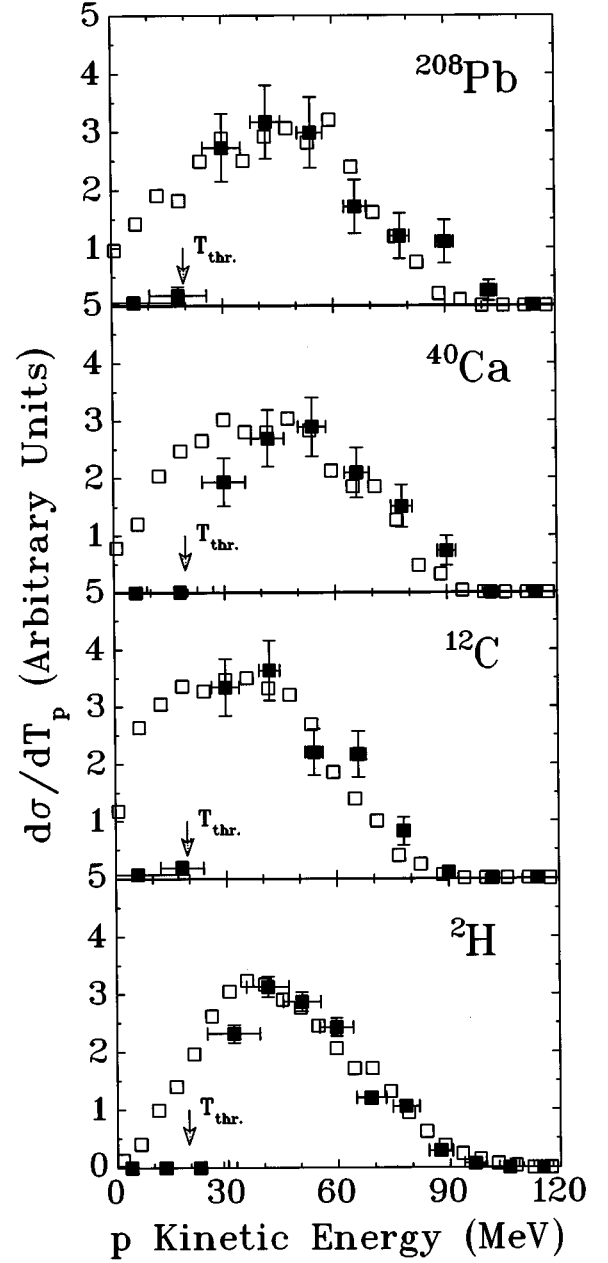


FIG. 6. Proton kinetic energy distributions in arbitrary units. The full squares correspond to the observed protons in the  $A(\pi^+, \pi^+ \pi^- p)[A-1]$  reaction. The proton energy is also derived [Eq. (3)] by measuring the kinetic energy of the two pions in the  $A(\pi^+, \pi^+ \pi^- p)[A-1]$  reaction (open squares). The arrows indicate the CHAOS threshold for protons.

distributions  $\mu_{E_M}$ . For  ${}^2\text{H}$  and  ${}^{12}\text{C}$ ,  $\sigma_{E_M}^i$  accounts for most of the observed width of the  $E_M$  distribution, in accord with the assumption that  $[A-1]$  stays bound throughout the reaction. In the case of  ${}^{40}\text{Ca}$  and  ${}^{208}\text{Pb}$ ,  $\sigma_{E_M}$  is somewhat larger than  $\sigma_{E_M}^i$ . For these nuclei, the residual nucleus is likely to de-excite through nucleon emission.

## IV. RESULTS AND DISCUSSIONS

### A. Recoil momentum

The recoil momentum distributions ( $p$ ) of the residual  $[A-1]$  system obtained from the present

$A(\pi^+, \pi^+ \pi^- p)[A-1]$  measurements are shown in Fig. 4. These distributions ( $d\sigma/dp$  in arbitrary units) show marked similarities to momentum density distributions  $\times p^2$  determined from studies of  $A(e, e'p)[A-1]$  reactions. We will rely on this fact when interpreting the present results. Thus, it is useful to recall some properties of the  $(e, e'p)$  process [14–16]: By measuring the momenta of the scattered electron and the ejected proton in an  $A(e, e'p)[A-1]$  reaction, one can determine the excitation energy and the recoil momentum of the residual  $[A-1]$  system. The  $A(e, e'p)$  reaction is quasifree. Therefore, in absence of distortions, the measured  $[A-1]$  recoil momentum distributions are the same as the momentum distributions of the ejected protons before the collision, and can be successfully compared with nuclear shell model calculations.

${}^2\text{H}$ . The solid line in Fig. 4 is the momentum density distribution  $\times p^2$  measured by Ref. [14] for the  ${}^2\text{H}(e, e'p)n$  reaction. The full squares indicate the momentum distribution measured presently. The two distributions (in arbitrary units) show the same behavior: the unobserved nucleon in the two reactions  ${}^2\text{H}(\pi^+, \pi^+ \pi^- p)p$  and  ${}^2\text{H}(e, e'p)n$  recoils with the same momentum, which corresponds to the nucleon Fermi motion. This is the first direct observation of the quasifree nature of the pion production process [17], which is accounted for by the  $\pi N \rightarrow \pi \pi N$  elementary reaction.

${}^{12}\text{C}$ . The measured recoil momentum distribution for the  ${}^{12}\text{C}(\pi^+, \pi^+ \pi^- p)$  reaction is represented by full squares. The curves are the result of distorted wave impulse approximation (DWIA) calculations for the  ${}^{12}\text{C}(e, e'p)$  reaction [15] for protons knocked out from the  $1p_{3/2}$  and  $1s_{1/2}$  orbitals. The two curves are normalized to the present data by constraining their areas to have the same ratio as the areas subtended by the Gaussian peaks in Fig. 5. Within this approach, the initial  $\pi^+ n \rightarrow \pi^+ \pi^- p$  reaction occurs 85% of the time on  $1p_{3/2}$  neutrons and 15% of the time on  $1s_{1/2}$  neutrons. More detail will be given when discussing Fig. 5.

${}^{40}\text{Ca}$  and  ${}^{208}\text{Pb}$ . For these two nuclei the measured momentum distributions (full squares) show a similar behaviour: a peak at 40–60 MeV/c, followed by a broad distribution centered at about 180–200 MeV/c. Due to the moderate missing energy resolution of the experimental apparatus, and the large number of nuclear orbitals available, it is not possible to establish the yield of the initial  $\pi^+ n \rightarrow \pi^+ \pi^- p$  reaction from individual neutron orbitals. However, it is evident that almost all of the measured yield is at low recoil momenta, below 350 MeV/c. This is a feature which is commonly observed in quasifree reactions. For instance, for the  $(e, e'p)$  process, the missing momentum yield drops at  $\approx 250$  MeV/c [15,16].

The comparison of the recoil momentum distributions for the  $A(\pi^+, \pi^+ \pi^- p)[A-1]$  reaction and the equivalent quantity for the  $A(e, e'p)[A-1]$  reaction leads to the conclusion that the initial stage of the pion production reaction in nuclei is a quasifree process. i.e., it involves only one nucleon, and proceeds via the elementary  $\pi N \rightarrow \pi \pi N$  reaction, while the residual  $[A-1]$  nuclear system is left substantially undisturbed.

## B. Missing energy

The measured missing energy distributions are presented in Fig. 5, and discussed below. The full squares in Fig. 5

represent the results obtained from the full data set, while the open squares are for those events in which the invariant mass of the  $\pi^+ \pi^-$  pair in the final state is restricted to be below 315 MeV, which is the region in which an  $A$ -dependent enhancement has been reported [6].

${}^2\text{H}$ . For this nucleus, the reaction is  ${}^2\text{H}(\pi^+, \pi^+ \pi^- p)p$ , and the unobserved particle is a proton. Since the momenta of the three observed particles are measured, the mass of the undetected proton can be derived directly from the data. Hence, the  $m_p$  distribution is presented instead of the proton missing energy. The full line is a Gaussian fit to the data. The best-fit parameters are  $\mu = 938.9$  MeV and  $\sigma = 7.6$  MeV. The symmetry of the  $m_p$  distribution and its mean value, approximately equal to the proton mass of 938.3 MeV, demonstrate the reliability of both the measurement and the analysis.

${}^{12}\text{C}$ ,  ${}^{40}\text{Ca}$ , and  ${}^{208}\text{Pb}$ . For these nuclei the missing energy,  $E_M$ , has been calculated by assuming that the recoil nucleus is bound. The reactions studied are  $A(\pi^+, \pi^+ \pi^- p)[A-1]$ , and the recoil nuclei are  ${}^{11}\text{C}$ ,  ${}^{39}\text{Ca}$ , and  ${}^{207}\text{Pb}$ . The full lines in Fig. 5 are Gaussian fits to the data. The best-fit parameters ( $\mu_{E_M}$  and  $\sigma_{E_M}$ ) are listed in Table II. The choice of a Gaussian distribution to describe the data was suggested by the shape of the  $E_M$  distributions, which, in fact, all appear to be symmetric around their mean value.

The dashed curve in Fig. 5 shows the results of a phase-space simulation of the  ${}^{40}\text{Ca}(\pi^+, \pi^+ \pi^- p)p$  reaction. This represents the missing energy distribution one might expect to obtain if more than one nucleon were involved in the pion production process. Evidently, both the shape and the centroid of this simulated  $E_M$  distribution are different from the observed one. Simulations for other nuclei yield similar results. They also predict large values of missing momentum (up to 1 GeV/c), which are not observed in the momentum distributions presented in Fig. 4.

The carbon missing energy is best fit by a sum of two Gaussian distributions, with centroids at 5.0 and 37.7 MeV. This latter value is comparable to  $\approx 35$  MeV, which is the mean value of the  $1s$ -hole strength distribution in the  ${}^{12}\text{C}(e, e'p)$  reaction [15]. The areas under the two distributions indicate the relative probabilities for the initial  $\pi^+ n \rightarrow \pi^+ \pi^- p$  reaction to take place either on a  $1p_{3/2}$  or a  $1s_{1/2}$  orbital of  ${}^{12}\text{C}$ . The ratio between the two areas is  $5.6 \pm 0.7$ , which leads to a probability for the elementary reaction to occur on a  $1p_{3/2}$  orbital of 85% and on a  $1s_{1/2}$  orbital of 15%. For calcium and lead a second peak at 35–40 MeV is not observed. This implies that the probability of neutron removal from internal nuclear orbitals is below 15%.

These observations lead to the conclusion that the nucleon involved in the pion production process is likely to belong to external nuclear orbitals, regardless of  $A$ . The relatively small amount of observed missing energy is accounted for by  $E_{A-1}^*$ , and thus leads to the additional conclusion that the detected  $\pi^+ \pi^-$  pairs release a negligible fraction of their kinetic energy to the nucleus. The same applies to the observed proton.

It is to be noted that the  $E_M$  distributions represented with the open squares in Fig. 5 are not significantly different, apart from a scale factor, from the ones represented by the

full squares. Thus, the conclusions drawn above for the full data set can be reasonably extended to the subset of the data in which the  $\pi^+\pi^-$  invariant mass is limited to the range  $2m_\pi < M_{\pi^+\pi^-} < 315$  MeV.

### C. Proton energy

In the pion-induced pion production reaction on nuclei, the proton energy can be determined directly by detecting the proton in the final state, or calculated from the energies of the two detected pions, under the assumptions that the reaction is quasifree, and that the residual nucleus is left in its ground state. In the former case, the measured proton energy distributions will be affected by the CHAOS threshold. In addition, they will reflect any energy losses suffered by the outgoing protons in collisions with the nucleons of the residual nucleus. Such energy losses are commonly defined as hard final state interactions (HFSI). In this article, HFSI is distinct from a final state interaction which arises when the outgoing particle loses some of its energy by interacting with the nuclear potential, and leaves the residual nucleus in some low-lying excited states. This type of FSI is accounted for by  $E_{A-1}^*$ . In the latter case, the calculated proton energy distributions are not altered either by proton HFSI's or the CHAOS threshold. They represent the proton kinetic energy at the production stage, provided the  $\pi^+\pi^-$  pair releases a negligible fraction of its kinetic energy on the way out from the nucleus.

<sup>2</sup>H. The two proton energy distributions are reported in Fig. 6. The full and open squares correspond to the observed and unobserved proton, respectively. The two distributions coincide up to the CHAOS threshold, as they should, since, for this nucleus, proton and pion HFSI's are negligible.

<sup>12</sup>C, <sup>40</sup>Ca, and <sup>208</sup>Pb. For these nuclei the shape of the observed proton (full squares) in the  $A(\pi^+, \pi^+\pi^-)[A-1]$  reaction also coincides, within the error bars, with the energy distribution of the unobserved proton (open squares) in the  $A(\pi^+, \pi^+\pi^-)p[A-1]$  reaction up to the CHAOS threshold. This indicates that the role of HFSI's is minimal for the present data set, regardless of nuclear mass number. This observation is consistent with the previous finding that the initial  $\pi^+n \rightarrow \pi^+\pi^-p$  reaction occurs preferentially on an external nuclear orbit.

## V. CONCLUSIONS

The pion-induced pion production reaction in <sup>2</sup>H, <sup>12</sup>C, <sup>40</sup>Ca, and <sup>208</sup>Pb has been studied with the  $A(\pi^+, \pi^+\pi^-)$  and, for the first time, the  $A(\pi^+, \pi^+\pi^-)p$  reactions at an incident pion energy of  $T_{\pi^+} = 282.7$  MeV. The pion production channel ( $\pi^+, \pi^+\pi^-$ ) was uniquely identified by detecting (at least) the pair of outgoing pions in coincidence with

the incoming pion. Kinematic quantities such as the missing momentum, the missing energy, and the proton kinetic energy have been extracted from the data set and used to determine the general features of the pion production reaction in nuclei. A consideration of the distributions of these quantities has led to the following *model-independent* conclusions: (1) The  $\pi \rightarrow \pi\pi$  reaction in nuclei is a *quasifree* process, involving a single nucleon, and proceeding via  $\pi N \rightarrow \pi\pi N$ . (2) The interacting nucleon preferentially lies in an external nuclear orbital. (3) The residual  $[A-1]$  nucleus is only weakly perturbed by the pion production process. (4) The final pion pair propagates through the nucleus with no appreciable energy loss. Also, the observed proton in the  $A(\pi^+, \pi^+\pi^-)p[A-1]$  reaction releases a negligible amount of energy to the residual nucleus through HFSI's. These conclusions should be considered as input to new models addressing the dynamics of pion production in nuclei [18], and provide a means for testing the validity of existing models [19].

Recent results from pion production [5,6] have reported of a marked enhancement in the  $\pi\pi$  invariant mass with increasing  $A$ , in the range  $280 < M_{\pi\pi} < 315$  MeV, for  $I=J=0$  interacting pairs. In the present analysis,  $E_M$  distributions for events with the invariant mass of the detected pion pairs constrained to this range have been studied, and compared with the  $E_M$  distributions for unconstrained events. The two distributions display the same behavior, and thus the same conclusions can be drawn for both the constrained and unconstrained events. This can serve to eliminate some possible explanations of the observed  $M_{\pi^+\pi^-}$  enhancement. It cannot be due to an  $A$  dependence in the initial stage of the pion production reaction, or to HFSI's. At the energy of this experiment, the pion production cross section decreases sharply with the decreasing incident pion energy [19], and thus it is unlikely that hard initial state interactions distort the  $M_{\pi^+\pi^-}$  distributions near the  $2m_\pi$  threshold. The only part of interaction remaining is the  $(\pi\pi) - [A-1]$  interaction. Therefore, the observed enhancement of the  $M_{\pi^+\pi^-}$  distributions near the  $2m_\pi$  threshold with increasing  $A$  must be understood by studying the nuclear-medium modifications on the  $\pi$ - $\pi$  correlations.

## ACKNOWLEDGMENTS

The authors acknowledge the technical and financial support received from TRIUMF. The present work was made possible by grants from the Istituto Nazionale di Fisica Nucleare (INFN) of Italy, the National Science and Engineering Research Council (NSERC) of Canada, the Australian Research Council, and the California State University Sacramento (CSUS) Foundation.

[1] Yu. A. Batusov, S. A. Bunyatov, N. Dalkhazhav, G. Ionice, E. Losneanu, V. Mihul, V. M. Sidorov, D. Tuvdendorzh, and V. A. Yarba, *Sov. J. Nucl. Phys.* **9**, 221 (1969).  
 [2] N. Grion *et al.*, *Nucl. Phys.* **A492**, 509 (1989); R. Rui *et al.*, *ibid.* **A517**, 455 (1990); D. Vetterli *et al.*, *ibid.* **A548**, 541 (1992); F. Bonutti, P. Camerini, N. Grion, R. Rui, D. Vetterli,

and F. M. Rozon, *Phys. Rev. C* **47**, 863 (1993).  
 [3] N. Grion *et al.*, *Phys. Rev. Lett.* **59**, 1080 (1987).  
 [4] A. Rahav *et al.*, *Phys. Rev. Lett.* **66**, 1279 (1991).  
 [5] P. Camerini, N. Grion, R. Rui, and D. Vetterli, *Nucl. Phys.* **A552**, 451 (1993).  
 [6] F. Bonutti *et al.*, *Phys. Rev. Lett.* **77**, 603 (1996).

- [7] A comprehensive treatment of this matter can be found in, T. Ericson and W. Weise, *Pions and Nuclei* (Clarendon, Oxford, 1988).
- [8] G. Chanfray, Z. Aouissat, P. Schuck, and W. Nörenberg, *Phys. Lett. B* **256**, 325 (1991); V. Mull, J. Wambach, and J. Speth, *ibid.* **286**, 13 (1992); Z. Aouissat, R. Rapp, G. Chanfray, P. Schuck, and J. Wambach, *Nucl. Phys.* **A581**, 471 (1995).
- [9] N. Grion and R. Rui, Measurements of the  $\pi^+\pi^-$  invariant mass in nuclei. A tool for determining the mass distributions of the  $\sigma$ -meson, TRIUMF Research Proposal 653, 1991.
- [10] G. R. Smith *et al.*, *Nucl. Instrum. Methods Phys. Res. A* **362**, 349 (1995).
- [11] G. J. Hofman, J. T. Brack, P. A. Amaudruz, and G. R. Smith, *Nucl. Instrum. Methods Phys. Res. A* **325**, 384 (1993).
- [12] F. Bonutti, S. Buttazzoni, P. Camerini, N. Grion, and R. Rui, *Nucl. Instrum. Methods Phys. Res. A* **350**, 136 (1994).
- [13] K. J. Raywood, P. A. Amaudruz, S. McFarland, M. E. Sevier, and G. R. Smith, *Nucl. Instrum. Methods Phys. Res. A* **357**, 296 (1995).
- [14] M. Bernheim, A. Bussierre, J. Mougey, D. Royer, D. Tarnowski, S. Turck-Chieze, S. Frullani, G. P. Capitani, D. De-Sanctis, and E. Jans, *Nucl. Phys.* **A365**, 349 (1981).
- [15] S. Frullani and J. Mougey, *Advances in Nuclear Physics* (Plenum, New York, 1983), Vol. 14.
- [16] I. Bobeldijk *et al.*, *Phys. Rev. Lett.* **73**, 2684 (1994); *Phys. Lett. B* **353**, 32 (1995).
- [17] Indirect observations of the quasifree nature of the  $\pi\rightarrow\pi\pi$  process on  $^2\text{H}$  are reported in, C. W. Bjork *et al.*, *Phys. Rev. Lett.* **44**, 62 (1980); R. Rui *et al.*, *Nucl. Phys.* **A517**, 455 (1990); V. Sossi *et al.*, *ibid.* **A548**, 562 (1992).
- [18] M. Vicente-Vacas and one of us, P. Camerini, are jointly working on a model for the  $^2\text{H}(\pi^+, \pi^+\pi^\pm)NN$  reaction which is based on the Oset's  $p(\pi^-, \pi^+\pi^-)n$  model [19]. Then, the underlying diagrams of this reaction will be extended to Oset's model for the  $A(\pi^+, \pi^+\pi^\pm)A'$  reaction [19]. Both models will incorporate the kinematic limits of CHAOS. In addition, G. Chanfray is being helped by F. Bonutti to include the in-medium effects on the  $\pi\pi$  interaction [8] into the Oset's model.
- [19] J. M. Eisenberg, *Phys. Lett.* **93B**, 12 (1980); R. M. Rockmore, *Phys. Rev. C* **27**, 2150 (1983); J. Cohen and J. M. Eisenberg, *Nucl. Phys.* **A395**, 389 (1983); R. M. Rockmore, *Phys. Rev. C* **29**, 1534 (1984); E. Oset and M. Vicente-Vacas, *Nucl. Phys.* **A446**, 584 (1985); E. Oset and M. Vicente-Vacas, *ibid.* **A454**, 637 (1986).